Space-time matrix model of power flow in SI-POFs applied to localized spatial disturbances

M.A. Losada[1], **J. Mateo**[1], **M. Osta**[1]

[1] *Group of Photonic Technology, Aragón Institute of Engineering Research (i3A), Universidad de Zaragoza, Zaragoza, Spain,*
alosada@unizar.es, jmateo@unizar.es

Abstract: Our aim is to reveal the potential of the matrix approach of the power flow equation to study the effects of devices such as scramblers, tappers, etc., over light propagation in plastic optical fibers. Here we devise an experimental method to characterize a particular scrambler as a matrix which can be directly introduced into the model framework to predict propagation properties. Thus, fiber bandwidth versus length was simulated for different scrambler configurations and then compared with experimental data to verify the characterization method and to derive important aspects of its impact on transmission.

Introduction. We recently proposed a fast and robust method to solve the power flow equation generalized to incorporate the temporal dimension and where fiber diffusion and attenuation are functions of the propagation angle.[1,2] The method provides the space-time optical power distribution with length from which angular power distribution, attenuation, bandwidth and pulse spreading can be derived. We have shown that model simulations reproduce experimental measurements of different POF parameters such as far field patterns and frequency responses.[3] In addition, the method allows us to predict some fiber propagation properties where it is difficult or unpractical to measure them. The method also offers a flexible tool to study the effects of the use of different devices, such as scramblers, tappers, etc, that can be characterized by modeling them as two-dimensional matrices to be introduced in our framework.

In fact, here we characterize a particular scrambler designed to obtain an overfilled launch or to increase the system bandwidth by filtering out modes at the receiver end.[4] We use short segments of plastic optical fibers of large numerical aperture (NA) and 1mm core diameter and insert the scrambler near its output end. We extract the angular output power profiles from the far field patterns measured as a function of the input angle, with and without the scrambler. A comparison of both sets of data gives a complete assessment of the scrambler effects that can be used to build its characteristic matrix. This matrix can be introduced in our model to predict the global scrambler-fiber system behavior. These model predictions have been compared to our previous experimental estimates of bandwidths versus fiber length obtained using this same scrambler, revealing a good agreement.

Experimental methods. We have tested PMMA optical fibers of similar properties (1mm diameter and high NA) from three different manufacturers: ESKA-PREMIER GH4001 (GH) from Mitsubishi, HFBR-RUS100 (HFB) from Agilent, and PGU-FB1000 (PGU) from Toray. The scrambler used in our measurements has seven corrugations with a 6mm pitch, and a corrugation depth of 0.5mm. This scrambler was reported to achieve the same exit NA irrespective of the launching NA.[5]

We have designed a method to characterize the scrambler separately from the fiber propagation characteristics, using experimental radial profiles for short fibers obtained by launching a collimated source to scan the input angle in the horizontal plane. The scan of radial profiles is obtained first without the scrambler and then, with the scrambler near the fiber output end. In this way, the propagation effects are negligible and all the changes in the profiles are produced by the scrambler. The radial profiles are obtained from the far field patterns (FFPs) recorded for each input angle by a cooled CCD following the same method as in our previous works.[6] The set-up has been described in those works except for the injection module. This module consists on a He-Ne laser beam of 635nm directly injected into the fiber input end, which is placed on the center of a motorized rotary mount in order to vary the launching angle by computer control. The FFP images, obtained for input angles varied from -40º to 40º at 1º steps, were automatically registered and stored, using the same exposition time for the whole run. Before the measurement, a careful alignment of the laser beam and the fiber input end was performed manually, but the rest of the process was computer controlled.

Characterization of the scrambler in the framework of the matrix propagation model. The whole angular scan was obtained first for fiber segments of 1.25m without the scrambler. Then, the same fiber segment was tested but with the scrambler inserted at 10cm from its output end, without changing the other conditions (laser injection, starting angle, fiber position, etc). Measurements for the three fibers described above were obtained but only those for the PGU fiber are shown as an example in Figure 1. The left image shows the radial profiles obtained without scrambler, while the middle one, shows radial profiles when the scrambler was placed close to the output end. The right image shows radial profiles calculated using the scrambler model, described later. We have used an image representation to display all the profiles for the same fiber at different input angles in a single plot. In all images, each column represents the radial profile for the corresponding input angle as a function of the output angle on the vertical axis. The mirror images of the profiles, corresponding to negative output angles, are also shown for the sake of symmetry. Notice that the profiles for negative input angles have also been measured and are not exactly the same as those obtained for the positive angles. This variability reveals the difference from the ideally symmetric response. Both the output and the launching angles are given as fiber external angle in degrees. To enhance the visibility of the lower power values obtained for the scrambler at high input angles, all images have been submitted to a logarithm transform. Higher values are shown in lighter gray and lower in darker gray. The scales are the same for all images, so those measurements obtained with the scrambler are darker indicating power loss. The images show how, when using the scrambler, the power is spread over a wider range of output angles and thus, the narrow rings clearly visible in the left image obtained without the scrambler nearly disappear in the middle and rightmost ones.

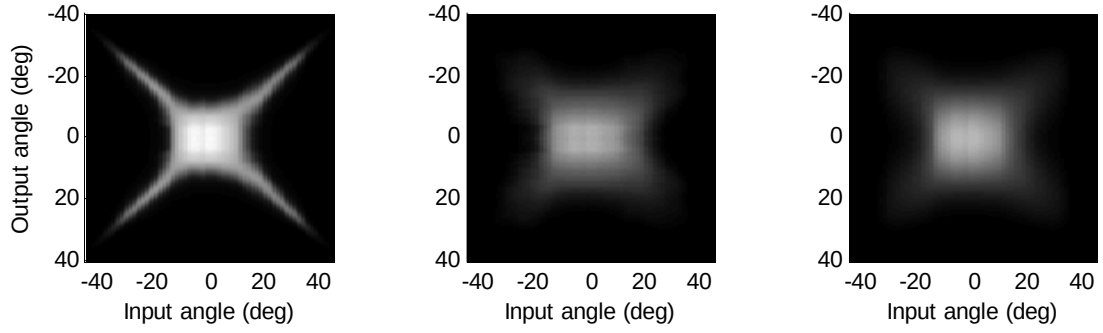

Fig. 1: Radial profile images for the PGU fiber: Leftmost image shows data without the scrambler; middle image shows data with the scrambler, and rightmost image shows data predicted by the scrambler model.

Following the matrix approach we proposed, we are going to model the scrambler as a matrix. Thus, given the input power profile as a column vector, $\boldsymbol{p_i}$, where each vector element is the power at a given angle, we assume that the scrambler behavior is linear and thus the output power vector, $\boldsymbol{p_o}$ can be obtained by matrix product of $\boldsymbol{p_i}$, by the scrambler characteristic matrix, **S**, given as $\boldsymbol{p_o} = \mathbf{S}\cdot\boldsymbol{p_i}$. The images presented above, showing compactly all radial profiles for different input angles, can be also seen as matrices where each column is a power vector whose horizontal index represents the input angle. Thus, the effects of the scrambler over the whole data set can be directly calculated as the matrix product: $\mathbf{P_o} = \mathbf{S}\cdot\mathbf{P_i}$, where $\mathbf{P_o}$ and $\mathbf{P_i}$ are matrices build as column power vector aggregates.

In matrix **S**, each column indicates the spread of the power in a given input angle due to the scrambler. Each element in the column gives the relative power transferred to the angle indicated by the row index. When power spread is independent on the input angle, all columns are shifted versions of the central one at 0º, and the matrix product is equivalent to a convolution of a single function by the input power vector. Then, we first tried to model the scrambler by a convolution with a single Gaussian function whose width and height were fitted using the data for the whole angular scan, but we were unable to obtain a good enough resemblance to our measurements. Thus, we assumed that the spread is not the same for all input angles but increases as a function of input angle, which is equivalent to modeling the scrambler as a spatially-variant system. Therefore, we used a Gaussian whose standard deviation depends on the angle and was fitted independently for each fiber type. We found that, although not identical, the same set of parameter values can be used for all fibers without

significant increase of the standard error. However, we found that the Gaussian amplitude is a different function of the input angle for each fiber type. Thus, the scrambler matrix was separated into the product of two matrices: **M**, for the spatial spread, characteristic of the scrambler and independent on fiber type, and **L**, a diagonal matrix that gives the angular dependent loss and is different for each fiber type, being **S** = **L**·**M**. Matrix **M** is shown on the left in Figure 2 represented as an image. In the middle plot, the scrambler loss functions are shown for the three fibers. The rightmost image shows **S** for the PGU fiber, obtained as the product of **M**, and its corresponding **L**.

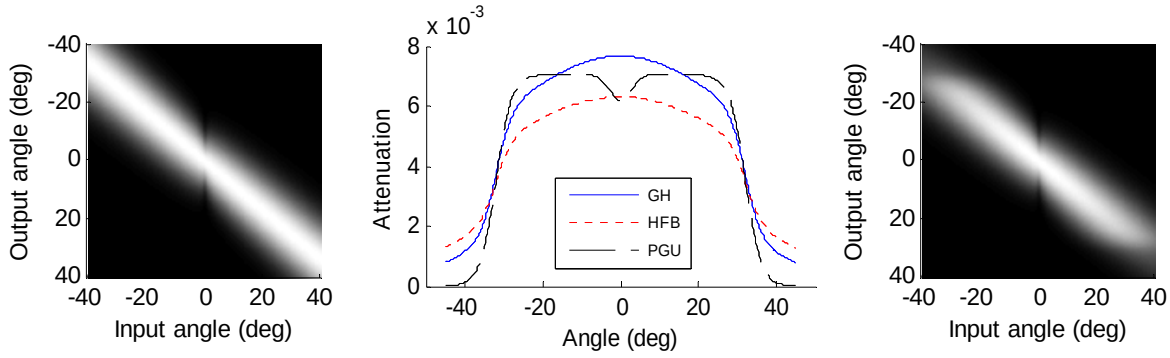

Fig. 2: Scrambler characteristic matrix. a) Image representation of matrix **M**. *b) Scrambler loss for the three fibers c) Matrix* **S** *calculated as the product of the* **L** *corresponding to the PGU fiber by matrix* **M**.

Discussion. We test the capability of our propagation model in matrix form to incorporate different localized effects, such as those produced for the scrambler under study. Gloge's power flow equation describes the evolution of the modal power distribution as it is transmitted throughout a POF where different modes are characterized by their propagation angle with respect to fiber axis (θ), considered as a continuous variable. Angular diffusion, $d(\theta)$, and attenuation, $\alpha(\theta)$, are described as functions of the propagation angle and are characteristic for each fiber type.[1-3] To solve this differential equation we implement a finite-difference method in a matrix form where for any pair of lengths, $z_2 > z_1$, we can put the difference equation in matrix notation as:

$$\boldsymbol{p}(z_2,\omega) = \big(\boldsymbol{A} + \boldsymbol{D}(\omega)\big)^m \cdot \boldsymbol{p}(z_1,\omega), \tag{1}$$

being $\boldsymbol{p}(z_1,\omega)$ and $\boldsymbol{p}(z_2,\omega)$ column vectors giving the angular power distribution in the frequency domain at two fiber lengths, whose difference is m-times the elementary length. **A** is a diagonal matrix that describes power propagation without diffusion, while the tri-diagonal matrix **D,** which is the only spatial frequency dependent term, accounts for fiber diffusion. These matrices are calculated from $\alpha(\theta)$ and $d(\theta)$ respectively, and thus, are different for each fiber type.[1-3]

This model, along with the characteristic matrix of the scrambler, **S**, is used to predict its effect on bandwidth versus fiber length. The effect of the scrambler is introduced as the right or left matrix product of **S** by the fiber propagation matrix, (**A**+**D**(ω)), depending whether the scrambler is at the transmitter or at the detector side respectively, such as the following equations show:

$$\boldsymbol{p}(z_2,\omega) = \big(\boldsymbol{A} + \boldsymbol{D}(\omega)\big)^m \cdot \boldsymbol{S} \cdot \boldsymbol{p}(z_1,\omega) \tag{2}$$

$$\boldsymbol{p}(z_2,\omega) = \boldsymbol{S} \cdot \big(\boldsymbol{A} + \boldsymbol{D}(\omega)\big)^m \cdot \boldsymbol{p}(z_1,\omega) \tag{3}$$

These predictions, obtained for the three fibers tested, are shown in Figure 3. The left plot shows the bandwidth versus length for the GH, the middle for the HFB and the right plot for the PGU. Dashed and solid lines show the model predictions for the scrambler at the input and output ends, respectively. For the sake of comparison, the dotted line shows the model prediction without scrambler.[3] Our results show that, when the scrambler is at the input end, the bandwidths are narrower than without the scrambler. When the scrambler is near the detector, however, its effect is a slight bandwidth increase. These effects are significant for fibers up to 50-60 meters, but for longer fibers the three conditions are similar. We have argued before that, when placed near the fiber input, the scrambler induces an angular spread producing a wide power distribution which then suffers fully the

diffusive effects of propagation. Near the detector, however, the scrambler acts as a spatial filter selectively losing power at the most delayed angles.[3,5]

In the same plots, experimental bandwidths versus length are also shown to compare them to the model predictions. These data were extracted from experimental frequency responses measured for the same fiber types analyzed here with the scrambler near the transmitter (squares) and with the scrambler near the detector (stars). The experimental procedure was based on the cut-back method, starting from long fiber samples down to 10m and was previously described in detail.[3,7] Frequency responses were also measured without the scrambler and were correctly reproduced by the propagation model as was previously published.[3,7] The plots show an overall agreement between the model and the experimental results, except for some discrepancies at short lengths which can be accounted for by some inherent variability in the measurement conditions such as changes in the scrambler insertion, fiber curvatures or defects, etc. Anyway, we have demonstrated the good performance of the matrix form of the power flow model to accommodate localized disturbance provided they can be properly characterized.

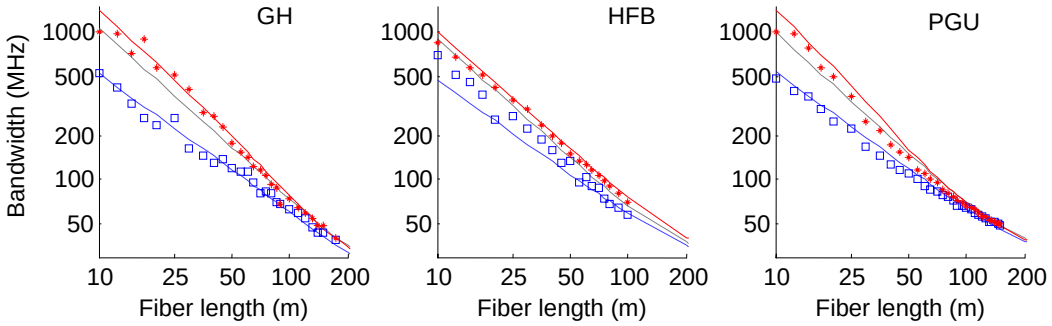

Fig. 3: Comparison of experimental and model predicted bandwidth versus length with the scrambler at the transmitter (squares and dashed line) and with the scrambler near the detector (stars and solid line). Model predictions of bandwidth without scrambler are shown as dotted lines.

Conclusions. We characterize a corrugated scrambler using experimental radial profiles measured by changing the input angle of a collimated beam. The scrambler can be modeled as the product of two matrices, one that describes power spread over adjacent angles, and a diagonal matrix that accounts for angular power loss. We found that the first matrix, describing power spread increase with input angle, is independent on fiber type. On the other hand, the scrambler angular loss is different depending on the fiber, as it can be related to cladding elasticity and manufacturing technique. Using the matrix propagation model, we predicted bandwidths introducing the scrambler near the input and output ends of the fibers. Thus, we confirm our previous experimental findings that the power spread caused by the scrambler near the transmitter decreases fiber bandwidth. However, the filtering effects produced by the scrambler near the detector result in a bandwidth increase. The extent of both effects depends on the fiber characteristics described by its diffusion and differential attenuation. We have demonstrated how the matrix power flow equation can be used, not only to model propagation, but can also be extended to introduce localized spatial disturbances in a compact and simple way.

Acknowledgements: This work was supported by the Spanish Ministry for Science and Technology under grant TEC2006-13273-C03-02.

References

1. J. Mateo, M. A. Losada, I. Garcés, Opt. Express 14, pp. 9028–9035, (2006).
2. F. Breyer, N. Hanik, S. Lee, S. Randel, Verlag Books on Demand GmbH, Norderstedt, (2007).
3. J. Mateo, M. A. Losada, J. Zubia, Opt. Express 17, pp. 2850–2860, (2009).
4. D. Kalymnios, in 8th Intl. Conf. on Plastic Optical Fibres and Applications, pp. 18–24, (1999).
5. J. Mateo, M. A. Losada, I. Garcés, J. Arrúe, J. Zubia, D. Kalymnios, in *12th Intl. Conf. on Plastic Optical Fibres and Applications*, pp. 123–126, (2003).
6. M. A. Losada, J. Mateo, D. Espinosa, I. Garcés, J. Zubia, in *13th Intl. Conf. on Plastic Optical Fibres and Applications*, pp. 458–465, (2004).
7. J. Mateo, M. A. Losada, J. J. Martínez-Muro, I. Garcés, J. Zubia, in *14th Intl. Conf. on Plastic Optical Fibres and Applications*, pp. 53–56, (2005).